Single-differential and integral cross sections for electron-impact ionization for the damage of carbon clusters irradiated with x-ray free-electron lasers

Takeshi Kai

Quantum Beam Science Directorate, Japan Atomic Energy Agency, 8-1 Umemidai Kizugawa-city, Kyoto 619-0215, Japan

(Received 25 June 2009; published 5 February 2010)

Single-differential and integral cross sections for electron-impact ionization of the C atom and its ions were calculated with the binary-encounter-dipole model [Y.-K. Kim and M. E. Rudd, Phys. Rev. A **50**, 3954 (1994)] to study the distribution of free-electron energies in carbon clusters after being irradiated with an x-ray free-electron laser (XFEL). The averaged energies of the secondary electrons for the C atom, and C^{1+}, C^{2+}, and C^{3+} ions were about 20, 70, 160, and 200 eV, respectively, when incident electron energy was about 20 keV, while those energies were in the order of tens of electronvolts when the incident electron energy was about 250 eV. The damage to carbon clusters irradiated with the XFEL was also investigated with time-dependent rate equations, considering photoionization, Compton scattering, Auger decay, and electron-impact ionization of the C atom and its ions. The results show that the electron-impact ionization becomes a more important process as the x-ray flux decreases, while the effect of Auger decay gradually appears as the x-ray flux increases. The energy dependence of the incident x ray was also investigated to evaluate the resolution of the diffraction pattern. These results indicate that we should make the XFEL pulse a few fs and about 16 keV to suppress damage and obtain desired resolution of the diffraction pattern.

DOI: 10.1103/PhysRevA.81.023201 PACS number(s): 36.40.−c, 34.50.Fa, 32.80.Fb

I. INTRODUCTION

Improvement of three-dimensional structural analysis of biomolecules is one of the critical issues in biology. The structure determination of biomolecules has been performed using the x-ray crystallography analysis, etc. However, making the sample crystal needed for x-ray crystallography analysis becomes very difficult with increase in the size of the single biomolecule being studied. To investigate a possible way to determine the structure of the single biomolecules [1], x-ray free-electron lasers (XFEL) are being developed in the European Union, United States, and Japan and will be completed around 2010 [2–4]. For this measurement, a large number of x-ray photons may be necessary. The target samples, however, are damaged by photoionization, Auger decay, Compton scattering, and electron-impact ionization processes that are caused by high intense x-ray irradiation [5–14]. It might be very difficult to carry out the reconstruction of a highly damaged sample. In addition, the existence of the free electrons in a biomolecule influences the diffraction pattern, producing noise. To understand these serious problems in detail, we must estimate the damage caused by those atomic processes that influence the diffraction patterns.

Here, we concentrate on describing the atomic processes leading to damage of a biomolecule. The photoionization process and the Compton scattering are directly caused by high intense x rays. Therefore, we call those processes "primary damage." The Auger decay and the electron-impact ionization processes are here called "secondary damage" because they are indirectly processes caused by the x-ray photons. In pioneering reports on these atomic processes [5,6], electron-impact ionization was not considered because a smaller target such as a lysozyme molecule (2643 atoms) was adopted [5], while the Compton scattering was not considered because an x-ray wavelength of ∼0.1 nm (or energy of ∼12 keV) was a simulation condition [6]. Their article [6] pointed out the importance of electron-impact ionization, using a thermalized Maxwellian electron distribution function. And they assumed that the energies of secondary (or ejected) electrons of carbon atoms and ions created by electron impact were approximately three times its average ionization energy, or about 25 eV. Ziaja *et al.* [15] described the energy of secondary electrons produced by electron impact in a diamond target using a formula of the Lindhard dielectric function. Their results showed that the energies were less than 100 eV. In recent years, Caleman *et al.* [16] studied electron properties and electron-impact ionization in crystalline urea ($CO(NH_2)_2$).

In the present study, the photoionization, the Auger decay, the Compton scattering, and the electron-impact ionization were all taken into account in a parameter survey of pulse widths and energies in the x-ray region. In addition, we addressed the electron-impact ionization and the energy distribution of free electrons in the biomolecules. When a biomolecule is irradiated with an XFEL with photon energy of 12 keV, free electrons of different energy components (∼12 keV are photoelectrons, ∼250 eV are Auger electrons [5], and ∼270 eV are Compton recoil electrons) are created in the biomolecule. Therefore, to determine causes of the damage, the energies of the secondary electrons produced by the processes listed above were also estimated.

We performed this parameter survey to study the damage to carbon clusters irradiated with XFEL under some of the conditions of previous reports [13,14]. In this article, we perform the parameter survey of the damage in more detail. A one-dimensional spherical model was used to study the damage to biomolecules irradiated with an XFEL [6,11,13,14]. We assumed that the target biomolecules can be treated as carbon clusters with radius r and solid density $\sim 3 \times 10^{22}$ atoms/cm^3. For the parameter survey of the damage to a carbon cluster (r 10 nm), time-dependent rate equations for the atomic processes of the C atom and its ions were solved. We selected conditions in which the x-ray energy ranged from 6 to 20 keV and the pulse width ranged from 1 to 10 fs, and we defined

the time-averaged number of bound electrons of carbons in the cluster to discuss the damage easily. The contributions of the previously mentioned atomic processes to ionization were investigated with x-ray flux from 1×10^{19} to 1×10^{22} photons/(pulse mm^2). The resolution of the diffraction pattern is dependent on the incident x-ray energy [17]. We also investigated the energy dependence of the incident x ray to evaluate the resolution of the diffraction pattern. Finally, we describe the results of this parameter survey of the damage to carbon clusters, the x-ray flux of elastic-scattering photons of the carbon cluster with the damage, and the energy dependence of the incident x ray.

II. THEORETICAL CALCULATIONS

For the electron-impact ionization process, several theoretical methods have been developed [18–21]. In this work, the binary-encounter-dipole model (BED) [20] based on the Rutherford cross section was employed to calculate the single-differential cross section (SDCS). The energy distributions and averaged energies of secondary electrons were obtained from the SDCS. The SDCS of the C atom and its ions are calculated by the BED model expressed by the equation

$$\frac{d\sigma}{dW} = \frac{S}{B(t+u+1)}\left\{\frac{N_i/N-2}{t+1}\left(\frac{1}{w+1}+\frac{1}{t-w}\right) + \left(2-\frac{N_i}{N}\right)\left[\frac{1}{(w+1)^2}+\frac{1}{(t-w)^2}\right] \times \frac{\ln t}{N(w+1)}\frac{df(w)}{dw}\right\}, \quad (1)$$

with

$$t = T/B, \quad w = W/B, \quad u = U/B,$$
$$S = 4\pi a_0^2 N (R/B)^2, \quad N_i = \int_0^\infty \frac{df(w)}{dw} dw,$$

where B is the binding energy of the ejected electron, T is the nonrelativistic kinetic energy of the incident electron, W is the kinetic energy of the ejected electron, $U = \langle p^2/2m \rangle$ is the orbital-electron-kinetic energy in terms of the target electron momentum $\vec{p}$ and the electron mass m, a_0 is the Bohr radius, and R is the Rydberg energy. In Eq. (1), $df(w)/dw$ is the differential-oscillator strength as a function of w. Hartree-Fock wave functions of the C atom and its ions [23] were used to calculate the orbital electron kinetic energy U. The differential-oscillator strengths of the C atom and its ions were calculated with the Flexible Atomic Code (FAC) [24]. The integral cross section (ICS) σ_{EI} and averaged energy of secondary electron $\langle W \rangle$ are given by

$$\sigma_{\mathrm{EI}} = \int_0^{(T-B)/2} \frac{d\sigma}{dW} dW, \quad (2)$$

and

$$\langle W \rangle = \frac{\int_0^{(T-B)/2} W \frac{d\sigma}{dW} dW}{\int_0^{(T-B)/2} \frac{d\sigma}{dW} dW}. \quad (3)$$

We note that the rate of electron-impact ionization should be employed, $n_e v_e \sigma_{\mathrm{EI}}$, since the free-electron distribution in the target cluster has not thermalized at ~10 fs (n_e and v_e are the electron density and velocity of each electron component, respectively). The photoionization cross sections σ_{PI} were calculated using the FAC [24]. The calculated cross sections were in good agreement with previous results of calculations based on the Manson-Cooper method [25]. For the Compton scattering of bound electrons, we must correct the cross section from the Klein-Nishina formula using the incoherent scattering function [26]. However, those results are roughly the same as the results of the Klein-Nishina formula in the x-ray region from 6 to 20 keV [26]. In this article, the Compton cross sections σ_{CP} and Compton recoil electron energies were derived with the Klein-Nishina formula. Rates of the photoionization process and the Compton scattering were obtained by calculating $I\sigma_{\mathrm{PI(CP)}}/h\nu$, where I is the intensity (W/cm^2) of the x rays. Auger rates were taken from previous results [11].

In our atomic model, we addressed photoelectrons that escaped from or were trapped within the target sample. The photoelectrons generated in the target can go straight ahead in an arbitrary direction. We assumed that the photoelectrons travel on average from the center of the target forward to the outside. The photoelectrons can escape from the target cluster at first. Therefore, the target cluster is ionized if these photoelectrons collide with atoms within the target of radius r. After, the target gradually becomes positively charged and, finally, the photoelectrons will be trapped within the target clusters when the potential energy on the cluster surface is equal to the photoelectron energy. Under these conditions, the photoelectrons gradually accumulate in the target cluster. We assumed that the Compton recoil electrons, the Auger electrons, and secondary electrons were trapped in the target at all times, because their kinetic energies were sufficiently low.

In this work, an x-ray pulse with the energy of 6 ~20 keV was employed. The pulse had Gaussian distribution and a width of 1 ~10 fs. The time-dependent rate equation was solved using the above-mentioned atomic data and the following series of equations [11,13]:

$$\frac{dP_0(t)}{dt} = -\beta_0 P_0(t),$$
$$\frac{dP_1(t)}{dt} = \alpha_{0,1} P_0(t) - \beta_1 P_1(t),$$
$$\vdots$$
$$\frac{dP_n(t)}{dt} = \sum_m \alpha_{m,n} P_m(t) - \beta_n P_n(t),$$

where $P_i(t)$ is the population of the ground state or ionic state i of an atom or one of its ions such as singly inner-shell ionized atoms and hollow atoms, $\alpha_{m,k}$ is the transition rate from the mth to the kth state, and β_k is the total ionization rate (photoionization plus Auger decay plus collisional ionization plus Compton scattering) in the kth state. We defined the time-averaged number of bound electrons in a carbon cluster as

$$\langle N \rangle = \frac{\int \sum_i N_i P_i(t) I(t) dt}{\int I(t) dt}, \quad (4)$$

where N_i is the number of electrons in a subshell and $I(t)$ is x-ray flux. This flux plays a weight role in the time-average integral because both the elastic scattering needed for the

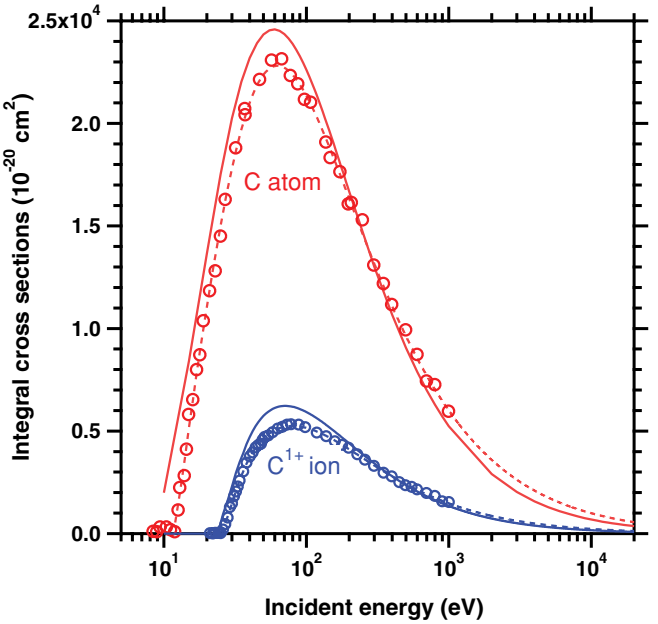

FIG. 1. (Color online) Ionization cross section of the C atom (C^{1+} ion) from the ground state to all the $1s^22s^22p$ and $1s^22s2p^2$ ($1s^22s^2$ and $1s^22s2p$) states. Lines in ascending order: red solid line, our calculations for the C atom; red dashed line, recommended data for the C atom [29]; red circles, experimental data for the C atom [27]; blue solid line, our calculations for the C^{1+} ion; blue dashed line, recommended data for the C^{1+} ion [29]; blue circles, experimental data for the C^{1+} ion [28].

diffraction pattern and the damage to the target are roughly proportional to x-ray flux evolving over time. Using the value of the time-averaged number of bound electrons $\langle N \rangle$, we can easily discuss the damage to a carbon cluster caused by varying values of pulse width and energy of the XFEL.

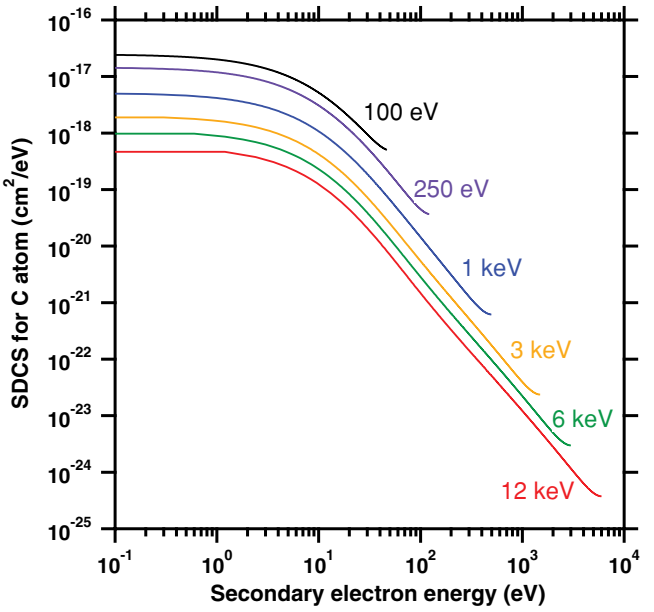

FIG. 2. (Color online) Single-differential cross sections of C atom for the $1s^22s^22p^2 \rightarrow 1s^22s^22p$ transition. Lines top to bottom: black line, incident electron energy of 100 eV; violet line, 250 eV; blue line, 1 keV; yellow line, 3 keV; green line, 6 keV; red line, 12 keV.

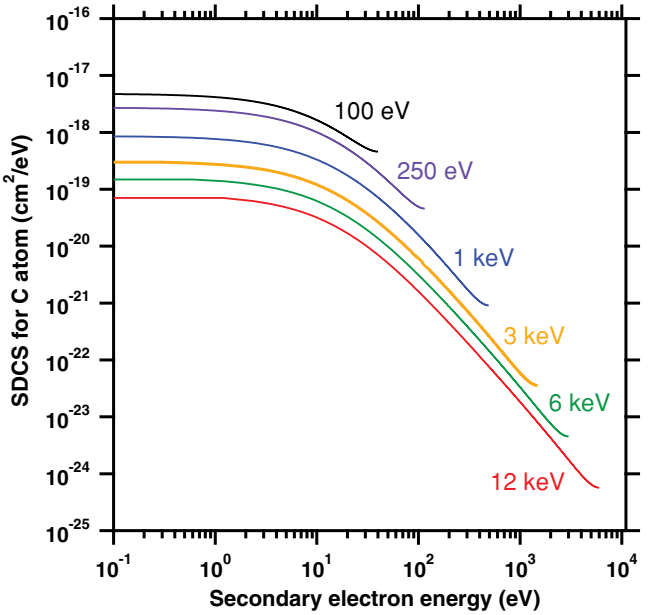

FIG. 3. (Color online) Single-differential cross sections of C atom for the $1s^22s^22p^2 \rightarrow 1s^22s2p^2$ transition. Lines top to bottom: black line, incident electron energy of 100 eV; violet line, 250 eV; blue line, 1 keV; yellow line, 3 keV; green line, 6 keV; red line, 12 keV.

III. RESULTS AND DISCUSSIONS

We calculated the ICS of a C atom and a C^{1+} ion using the BED model. Figure 1 compares our calculated results with the experimental results [27,28] and the recommended data [29]

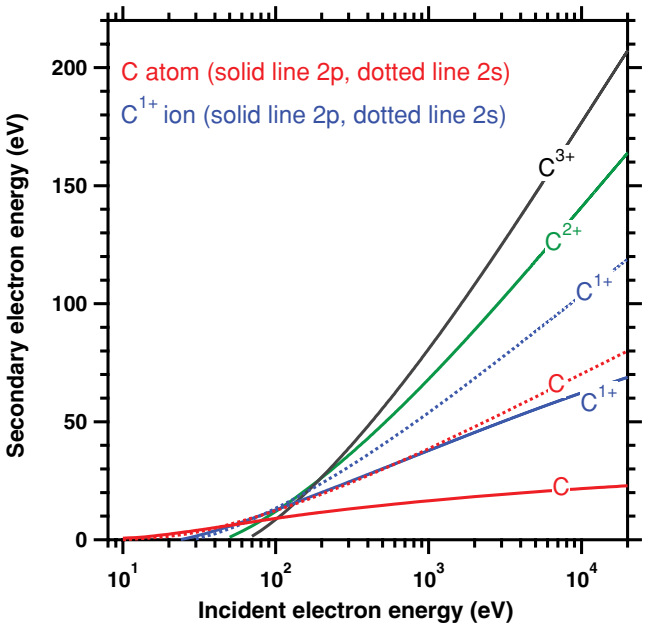

FIG. 4. (Color online) Averaged energies of secondary electron of C atom, C^{1+}, C^{2+}, and C^{3+} ions. Lines in ascending order: red solid line, $1s^22s^22p^2 \rightarrow 1s^22s^22p$ transition; red dotted line, $1s^22s^22p^2 \rightarrow 1s^22s2p^2$ transition; blue solid line, $1s^22s^22p \rightarrow 1s^22s^2$ transition; blue dotted line, $1s^22s^22p \rightarrow 1s^22s2p$ transition; green line, $1s^22s^2 \rightarrow 1s^22s$ transition; black line, $1s^22s \rightarrow 1s^2$ transition.

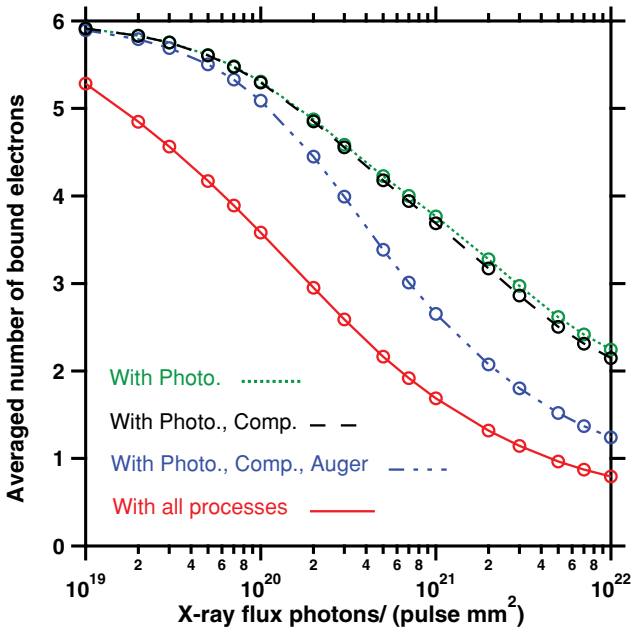

FIG. 5. (Color online) Averaged number of bound electrons of carbon clusters with x ray of pulse width 10 fs and energy 6 keV. Lines top to bottom: green line, with photoionization; black line, with photoionization and Compton scattering; blue line, with photoionization, Compton scattering, and Auger decay; red line, with all processes.

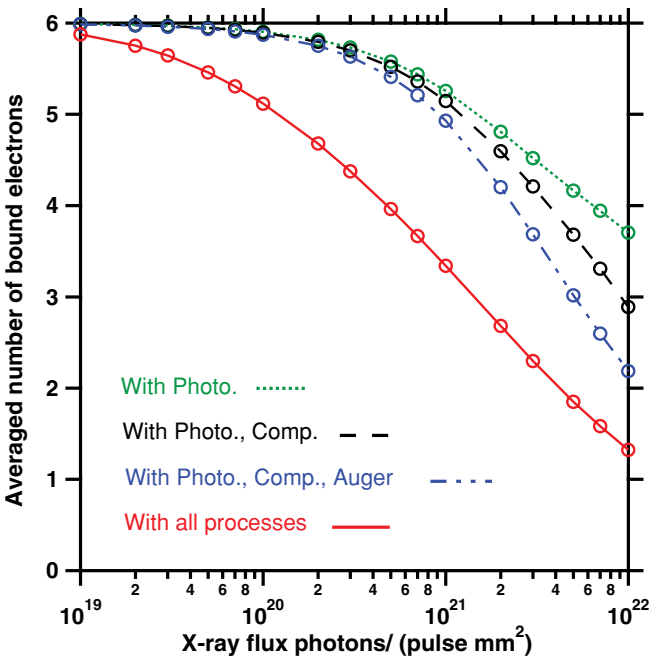

FIG. 6. (Color online) Averaged number of bound electrons of carbon clusters with x ray of pulse width 10 fs and energy 12 keV. Lines top to bottom: green line, with photoionization; black line, with photoionization and Compton scattering; blue line, with photoionization, Compton scattering, and Auger decay; red line, with all processes.

for a C atom and a C^{1+} ion from the ionization energy to 20 keV. Our results are in good agreement with the experimental results [27,28] and the recommended data [29]. Note that our calculations for other C ions using the BED model are also in good agreement with the recommended data [29]. To evaluate the calculations of the SDCS for a C atom and its ions, we calculated the SDCS of a He atom with incident electron energy of 100 eV, and compared this with previous theoretical and experimental results [22]. We confirmed that our calculations were in good agreement. Figure 2 shows our calculated SDCS of a C atom for the $1s^2 2s^2 2p^2 \rightarrow 1s^2 2s^2 2p$ transition in the cases of various incident electron energies. Figure 3 shows our calculated SDCS of a C atom for the $1s^2 2s^2 2p^2 \rightarrow 1s^2 2s 2p^2$ transition. It is seen from Figs. 2 and 3 that the electrons produced by electron impact are almost all low energy eve if the incident electron energy increased, since the SDCS drastically decreases with increase in the secondary electron energy.

We developed a calculation tool for the distribution of the secondary electron energy. However, it is difficult to include the calculated SDCS in this time-dependent rate equation. In this model simulation, the averaged energies of secondary electrons given by Eq. (3) are used. Figure 4 shows the calculated averaged energies of secondary electrons of a C atom, and of C^{1+}, C^{2+}, and C^{3+} ions. Those energies for the C atom, C^{1+}, C^{2+}, and C^{3+} ions are about 20 ($2p$-orbital ionized), 70 ($2p$-orbital ionized), 160 ($2s$-orbital ionized), and 200 ($2s$-orbital ionized) eV, respectively, with an incident electron energy of 12 keV (photoelectron impact). Those energies are in the order of tens of electronvolts when the incident-electron energy is about 250 eV (Compton-recoil and Auger-electron impact). Those results suggest that the ionization effects of the secondary electrons that are produced by Compton-recoil electron and Auger-electron impact also contribute to the damage of carbon cluster because the electron energies of the order of tens of eV may not be negligible from the collisional cross sections in Fig. 1. We hope that the present calculations of ICS, SDCS, and averaged energies of secondary electrons for the C atom and its ions will be applied to a detailed simulation [30–32] or another plasma simulation.

TABLE I. Upper limits for incident x-ray flux [photons/(pulse mm^2)]; $a[\pm b] = a \times 10^b$.

Pulse width	Incident x-ray energy						
	6 keV	8 keV	10 keV	12 keV	14 keV	16 keV	20 keV
1 fs	1.13[+20]	2.85[+20]	5.46[+20]	8.97[+20]	1.27[+21]	1.67[+21]	2.46[+21]
3 fs	6.52[+19]	1.72[+20]	3.23[+20]	5.18[+20]	7.12[+20]	9.43[+20]	1.36[+21]
5 fs	4.16[+19]	1.10[+20]	2.06[+20]	3.28[+20]	4.51[+20]	6.00[+20]	8.59[+20]
10 fs	1.58[+19]	4.10[+19]	7.67[+19]	1.24[+20]	1.77[+20]	2.36[+20]	3.43[+20]

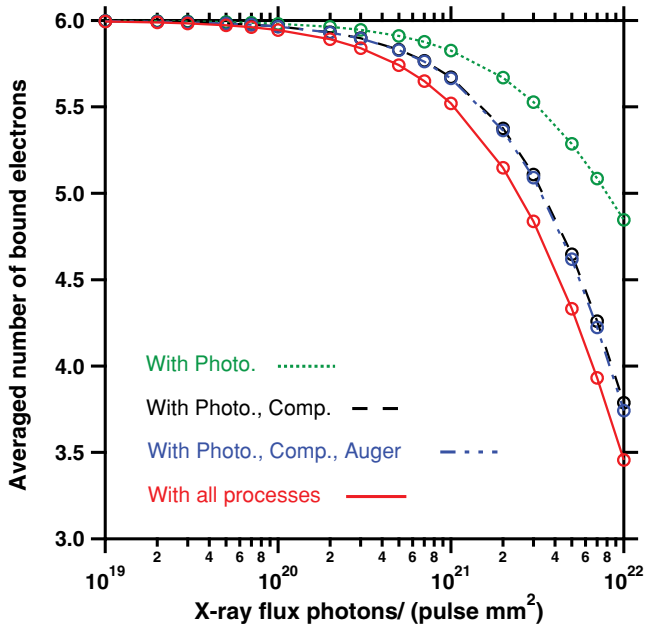

FIG. 7. (Color online) Averaged number of bound electrons of carbon clusters with x ray of pulse width 1 fs and energy 20 keV. Lines top to bottom: green line, with photoionization; black line, with photoionization and Compton scattering; blue line, with photoionization, Compton scattering, and Auger decay; red line, with all processes.

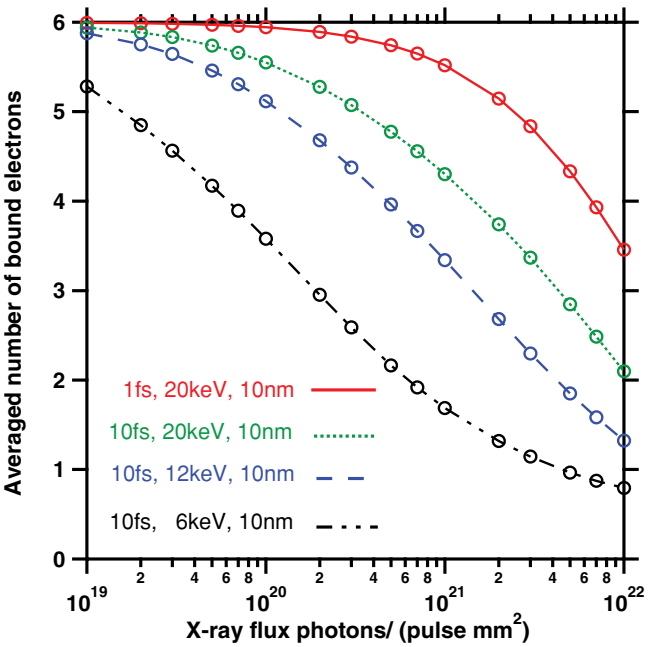

FIG. 8. (Color online) Averaged number of bound electrons of carbon clusters. Lines top to bottom: red line, x ray of pulse width 1 fs and energy 20 keV; green line, x ray of pulse width 10 fs and energy 20 keV; blue line, x ray of pulse width 10 fs and energy 12 keV; black line, x ray of pulse width 10 fs and energy 6 keV.

Time-dependent rate equations were solved to investigate the population dynamics of the C atom and its ions. Figures 5–7 show the the time-averaged number of bound electrons calculated using Eq. (4), as a function of x-ray flux photons/(pulse mm^2) in pulses of 10 fs and 6 keV, 10 fs and 12 keV, and 1 fs and 20 keV, respectively. The effect of photoionization decreases with increase in the x-ray energy since the photoionization cross section decreases in proportion to $E^{-3.5}$ [33], where the E is the photoelectron energy. We must select higher energy x rays to suppress the "primary damage." The degree of photoionization and Compton scattering is almost the same with x-ray energy of 20 keV, while the effect of the Compton scattering is very small with x-ray energy of 6 keV. We found that the electron-impact ionization became a more important process as the x-ray flux decreased, while the effect of Auger decay gradually appeared as the x-ray flux increased, because singly inner-shell ionized atoms and hollow atoms were gradually generated by higher intensity x rays. Figure 8 compares the calculated time-averaged number of bound electrons produced by different pulses. From Figs. 7 and 8, we see that the "secondary damage" due to the Auger decay and electron-impact ionization can be suppressed by selecting an XFEL of shorter pulse.

We will have to reconstruct the three-dimensional structure of a biomolecule from a diffraction pattern including the "primary" and "secondary" damage. We here briefly discuss the upper limit of intensity of XFEL for this structure determination. We assumed that the intensity of incident x ray became an upper limit when the averaged number of bound electrons was equal to 5.0. Table I shows that the upper limits of incident x-ray flux I_i [photons/(pulse mm^2)] in the x-ray energy ranged from 6 to 20 keV and the pulse width ranged from 1 to 10 fs. We must also discuss the intensity of diffraction pattern because the resolution of diffraction pattern is determined by the intensity of elastic-scattering photons. In the case of the experiment of a single biomolecule, the x-ray flux $I_0(k)$ [photons/(pulse pixel)] of elastic-scattering photons, which is unpolarized, can be approximated as follows [34]:

$$I_0(k) = I_i \frac{\sigma_T(k,\lambda)\lambda^2}{L^2} N_c f(k)^2, \tag{5}$$

TABLE II. Normalized x-ray flux of elastic-scattering photons; $a[\pm b] = a \times 10^b$.

Pulse width	Incident x-ray energy						
	6 keV	8 keV	10 keV	12 keV	14 keV	16 keV	20 keV
1 fs	5.10[−1]	7.24[−1]	8.88[−1]	1.01[+0]	1.05[+0]	1.05[+0]	1.00[+0]
3 fs	2.94[−1]	4.37[−1]	5.25[−1]	5.85[−1]	5.91[−1]	5.92[−1]	5.53[−1]
5 fs	1.88[−1]	2.79[−1]	3.35[−1]	3.70[−1]	3.74[−1]	3.77[−1]	3.49[−1]
10 fs	7.14[−2]	1.04[−1]	1.25[−1]	1.40[−1]	1.47[−1]	1.48[−1]	1.39[−1]

TABLE III. Average number of scattered photons [photons/(pulse pixel)]; $a[\pm b] = a \times 10^b$.

Pulse width	Momentum transfer of photon k (1/Å)						
	0.1	0.2	0.3	0.4	0.5	0.7	1.0
1 fs	5.88[−1]	4.92[−1]	3.76[−1]	2.72[−1]	1.92[−1]	1.02[−1]	5.27[−2]
3 fs	3.32[−1]	2.78[−1]	2.13[−1]	1.53[−1]	1.08[−1]	5.73[−2]	2.98[−2]
5 fs	2.11[−1]	1.77[−1]	1.35[−1]	9.76[−2]	6.89[−2]	3.65[−2]	1.89[−2]
10 fs	8.31[−2]	6.96[−2]	5.32[−2]	3.84[−2]	2.71[−2]	1.43[−2]	7.45[−3]

with

$$f(k) = \int_0^\infty 4\pi r^2 \rho_{\text{ion}}(r) \frac{\sin 2\pi kr}{2\pi kr} dr, k = \frac{2\sin\theta}{\lambda},$$

where k, λ, $\sigma_T(k,\lambda)$, L, N_c, and 2θ are momentum transfer of photon, wavelength of x ray, differential cross section of Thomson scattering, a molecular size, the number of atoms in the cluster, and scattering angle of photon, respectively. Then $f(k)$ and $\rho_{\text{ion}}(r)$ are atomic scattering factor and electron density of C^+ ion because the averaged number of bound electrons is equal to 5.0 in the carbon cluster. The electron density of C^+ ion was calculated from the Hartree-Fock wave functions given by Clementi and Roetti [23]. We calculated $I(k)$ in the x-ray energy ranged from 6 to 20 keV, the pulse width ranged from 1 to 10 fs, and the target radius was 10 nm. Then the values I_i of incident x-ray flux in Table I were used in those calculations. Table II shows the normalized x-ray flux of elastic-scattering photons at the momentum transfer 0.2 (1/Å) to investigate the x-ray energy dependence in previously mentioned XFEL conditions. Those values were normalized by the value in the pulse width 1 fs and x-ray energy 20 keV. We can see that the peak points of the x-ray flux of elastic-scattering photons are about 16 keV and the results of pulse width 10 fs roughly become one-seventh of the results of pulse width 1 fs from Table II. These results indicate that we should make the XFEL pulse a few fs and about 16 keV to suppress damage. Table III shows the average number of scattered photons using the values I_i of incident x-ray flux in Table I in the x-ray energy 16 keV, the pulse width ranged from 1 to 10 fs, and the target radius was 10 nm. In those cases, we found that the average number of scattered photons is less than one photon. We should use the method by which the three-dimensional structure of biomolecules can be reconstructed with one or less photons [34] to obtain the desired resolution.

IV. CONCLUSION

The photoionization, electron-impact ionization, and Compton scattering of the C atom and its ions were calculated using the FAC, the BED model, and the Klein-Nishina formula, respectively. We found that the averaged energies of secondary electrons of C atoms and C^{1+}, C^{2+}, and C^{3+} ions were about 20, 70, 160, and 200 eV, respectively, with an incident electron energy of 20 keV, while those energies were in the order of tens of electronvolts when the incident electron energy was about 250 eV. Time-dependent rate equations were solved to investigate the damage to the target sample. We also found that the electron-impact ionization became a more important process as the x-ray flux decreased, while the effect of Auger decay gradually appeared as the x-ray flux increased, and that "primary" and "secondary" damage to clusters can be suppressed by making the XFEL emit a shorter pulse and shorter wavelength. However, we found that the peak points of the x-ray flux of elastic-scattering photons were about 16 keV. In this article, we developed the simple atomic model for the damage of carbon cluster. For improvement of our model, it will be necessary to develop the detailed simulation code including electron and ions dynamics [5–9] and field ionization by strong internal electric field [12]. In the future, we will investigate the intensities of diffraction patterns derived together with the damage incurred by the biomolecules when we vary the values of various XFEL parameters in detail [10,35].

ACKNOWLEDGMENTS

We thank Professor N. Go and Drs. K. Moribayashi, H. Kono, A. Tokuhisa, J. Taka, T. Otobe, Y. Fukuda, T. Nakamura, and M. Yamagiwa for their useful discussion. This study was supported by the "X-ray Free Electron Laser Utilization Research Project" of the Ministry of Education, Culture, Sports, Science and Technology, Japan (MEXT).

[1] K. J. Gaffney and H. N. Chapman, Science **316**, 1444 (2007).
[2] The European X-Ray Laser Project [XFEL http://xfel.desy.de/].
[3] LCLS Project [http://www-ssrl.slac.stanford.edu/lcls/].
[4] SPring-8 Joint Project for XFEL, [http://www.riken.jp/XFEL/eng/index.html].
[5] R. Neutze, R. Wouts, D. van der Spoel, E. Weckert, and J. Hajdu, Nature **406**, 752 (2000).
[6] S. P. Hau-Riege, R. A. London, and A. Szoke, Phys. Rev. E **69**, 051906 (2004).
[7] G. Faigel, Z. Jurek, G. Oszlanyi, and M. Tegze, J. Alloys Compd. **401**, 86 (2005).
[8] S. P. Hau-Riege, R. A. London, H. N. Chapman, A. Szoke, and N. Timneanu, Phys. Rev. Lett. **98**, 198302 (2007).
[9] Z. Jurek and G. Faigal, Eur. Phys. J. D **50**, 35 (2008).

[10] S. P. Hau-Riege and H. N. Chapman, Phys. Rev. E **77**, 041902 (2008).
[11] K. Moribayashi, J. Phys. B: At. Mol. Opt. Phys. **41**, 085602 (2008).
[12] C. Gnodtke, U. Saalmann, and J. M. Rost, Phys. Rev. A **79**, 041201(R) (2009).
[13] K. Moribayashi and T. Kai, J. Phys: Conference series **163**, 012097 (2009).
[14] T. Kai and K. Moribayashi, J. Phys: Conference series **163**, 012035 (2009).
[15] B. Ziaja, R. A. London, and J. Hajdu, J. Appl. Phys. **97**, 064905 (2005).
[16] C. Caleman, C. Ortiz, E. Marklund, F. Bultmark, M. Gabrysch, F. G. Parak, J. Hajdu, M. Klintenberg, and N. Tîmneanu, Eur. Phys. Lett. **85**, 18005 (2009).
[17] M. R. Howells *et al.*, J. Electron Spectrosc. Relat. Phenom. **170**, 4 (2009).
[18] M. Inokuti, Rev. Mod. Phys. **43**, 297 (1971).
[19] S. Nakazaki, M. Nakashima, H. Takebe, and K. Takayanagi, J. Phys. Soc. Jpn. **60**, 1565 (1991).
[20] Y.- K. Kim and M. E. Rudd, Phys. Rev. A **50**, 3954 (1994).
[21] I. Bray and D. V. Fursa, Phys. Rev. A **54**, 2991 (1996).
[22] Y.- K. Kim, W. R. Johnson, and M. E. Rudd, Phys. Rev. A **61**, 034702 (2000).
[23] E. Clementi and C. Roetti, At. Data Nucl. Data Tables **14**, 177 (1974).
[24] M. F. Gu, Astrophys. J. **582**, 1241 (2003).
[25] J. J. Yeh and I. Lindau, At. Data Nucl. Data Tables **32**, 1 (1985).
[26] J. H. Hubbell, Wm. J. Veigele, E. A. Briggs, R. T. Brown, D. T. Cromer, and R. J. Howerton, J. Phys. Chem. Ref. Data **4**, 471 (1975).
[27] E. Brook, M. F. A. Harrison, and A. C. H. Smith, J. Phys. B: Atom. Molec. Phys. **11**, 3115 (1978).
[28] I. Yamada, A. Danjo, T. Hirayama, A. Matsumoto, S. Ohtani, H. Suzuki, T. Takayama, H. Tawara, K. Wakiya, and M. Yoshino, J. Phys. Soc. Jpn. **58**, 1585 (1989).
[29] H. Suno and T. Kato, At. Data Nucl. Data Tables **92**, 407 (2006).
[30] B. Ziaja, A. R. B. de Castro, E. Weckert, and T. Möller, Eur. Phys. J. D **40**, 465 (2006).
[31] B. Ziaja, H. Wabnitz, E. Weckert, and T. Möller, Eur. Phys. Lett. **82**, 24002 (2008).
[32] B. Ziaja, H. Wabnitz, E. Weckert, and T. Möller, New J. Phys. **10**, 043003 (2008).
[33] F. Khan, G. S. Khandelwal, and J. W. Wilson, J. Phys. B: At. Mol. Opt. Phys. **23**, 2717 (1990).
[34] G. Huldt, A. Szoke, and J. Hajdu, J. Struct. Biol. **144**, 219 (2003).
[35] S. P. Hau-Riege, Phys. Rev. A **76**, 042511 (2007).